

Scalable fabrication of single silicon vacancy defect arrays in silicon carbide using focused ion beam

Junfeng Wang,¹ Xiaoming Zhang,¹ Yu Zhou,¹ Ke Li,¹ Ziyu Wang,¹ Phani Peddibhotla,¹ Fucai Liu,² Sven Bauerdick³ and Axel Rudzinski,³ Zheng Liu,² and Weibo Gao^{1, 4, 5*}

¹*Division of Physics and Applied Physics, School of Physical and Mathematical Sciences, Nanyang Technological University, Singapore 637371, Singapore*

²*Center for Programmable Materials, School of Materials Science & Engineering, Nanyang Technological University, 50 Nanyang avenue, Singapore 639798, Singapore*

³*Raith GmbH, 44263 Dortmund, Germany*

⁴*The Photonics Institute and Centre for Disruptive Photonic Technologies, Nanyang Technological University, 637371 Singapore, Singapore*

⁵*MajuLab, CNRS-University of Nice-NUS-NTU International Joint Research Unit UMI 3654, Singapore*

**Corresponding author: wbgao@ntu.edu.sg*

Abstract

In this work, we present a method for targeted and maskless fabrication of single silicon vacancy (V_{Si}) defect arrays in silicon carbide (SiC) using focused ion beam. Firstly, we studied the photoluminescence (PL) spectrum and optically detected magnetic resonance (ODMR) of the generated defect spin ensemble, confirming that the synthesized centers were in the desired defect state. Then we investigated the fluorescence properties of single V_{Si} defects and our measurements indicate the presence of a photostable single photon source. Finally, we find that the Si^{++} ion to V_{Si} defect conversion yield increases as the implanted dose decreases. The reliable production of V_{Si} defects in silicon carbide could pave the way for its applications in quantum photonics and quantum information processing. The resolution of implanted V_{Si} defects is limited to a few tens of nanometers, defined by the diameter of the ion beam.

Silicon carbide (SiC) is a technologically mature semiconductor material, which can be grown as inch-scale high-quality single crystal wafers and has been widely used in microelectronics systems and high-power electronics, etc. In recent years, some defects in SiC have been successfully implemented as solid state quantum bit¹⁻⁸ and quantum photonics⁹⁻¹¹. They meet essential requirements for spin-based quantum information processing such as optical initialization, readout and microwave control of the spin state, which are similar as the nitrogen vacancy (NV) centers in diamond.¹² In particular, silicon vacancy (V_{Si}) defect in 4H-SiC has increasingly attracted attention owing to its excellent features, such as non-blinking single photon emission and long spin coherence times which persist up to room temperature (about 160 μ s).^{3,5,13} These remarkable properties have been exploited in many applications in quantum

photonics,^{9,10} and quantum metrological studies such as high sensitivity magnetic sensing^{14,15} and temperature sensing.¹⁶

The V_{Si} defect consists of a vacancy on a silicon site which exhibits a C_{3v} symmetry in 4H-SiC.^{3,5} In order to extend its applications in quantum information science, it is essential to develop the technique of scalable efficient generation of single V_{Si} defect arrays in 4H-SiC. Since the collected fluorescence rate of a single V_{Si} defect is modest with only about 10 kcps,^{3,5,17} it is required to couple with some photonic devices to improve the counts towards the construction of photonics networks.^{3,9,10,17,20} However, in order to realize the mode-maximum of photonic devices, it is necessary to place the V_{Si} defects relative to the optimal position with sub-wavelength-scale precision. Previously there are three methods to generate V_{Si} defect: the electron irradiation, neutron irradiation, and carbon implantation, however, these methods either can't control the position of the V_{Si} defect, or need a electron beam lithography (EBL) pre-fabricated photoresist patterned mask,^{3,5,9,17} which is not convenient for coupling to pre-fabricated photonic devices.

To solve this issue, in this work, we report a new approach to fabricate maskless and targeted single V_{Si} defects array in 4H-SiC using silicon focus ions beam implanted (FIB). This scalable post-fabrication approach can control the V_{Si} defect position accuracy in tens of nanometers, which can greatly simplify the design and fabrication process and improve the efficiency of V_{Si} defects based photonics structure fabrication.^{9,20} We used different dose (ions/spot) to create V_{Si} defect arrays and stripes (which serve as markers for reference) using 35 keV focused Si^{++} ions beam implantation. Firstly, we studied the room and cryogenic temperature photoluminescence (PL) spectrum and optically detected magnetic resonance (ODMR) of the ensemble defects on the stripe to confirm that they are V_{Si} defects. Then we studied the optical properties of a single V_{Si} defect in the lowest dose (40 Si/spot) area, and found it is a single photon source with good photo-stability. Moreover, we systematically investigate the mean counts per spot and the Si^{++} ion to V_{Si} defect conversion yield as a function of the implanted dose. Our results demonstrate that this method is well adapted to the targeted scalable generation of V_{Si} defects, paving ways towards V_{Si} defect based scalable quantum photonic devices.

A commercial 40 keV nanoFIB system (ionLINE Plus, RAITH Nanofabrication) was used for the focused Si ion beam implantation. The nanoFIB system creates a tightly focused ion beam with a diameter of a few nanometers from liquid metal alloy ion sources, which ensure the implanted Si ions lateral distribution at nanoscale. Moreover, it can also realize parallel Si ions implantation about tens of thousands of sites per second, which allows scalable fabrication of V_{Si} defects in the sample.²⁰ A commercial high-purity 4H-SiC sample with a low background fluorescence was used for the experiments.^{3,5,17} A 35keV double charged silicon ions (Si^{++}) were implanted onto the sample to generation V_{Si} defect array. The implantation spots were targeted with between 40 to 700 Si ions with a 5-10nm nanometers focus ion beam spot.¹⁹⁻²¹ Two stripes with their width about 1.5 μm was also generated by 700 Si ions/ spot (20nm step size in each direction), which were used for marking. The ion current was controlled by both the beam current and the

implantation time. After annealing the implanted defect array sample at 650 °C in air for 6 hours, we put the sample in HNO₃ for 24 hours to remove amorphous SiC layer in order to decrease the fluorescence background.³ The positioning accuracy of the V_{Si} defect is determined by the diameter of the focused ion beam (5-10nm) and the lateral straggling effects of implanted silicon ions in SiC. Inferred from SRIM simulations, the average depth of the silicon ions was 18.5nm, and its longitudinal and lateral straggling uncertainty was about 7 and 6 nm respectively. So it is estimated that the spatial positioning precision of the V_{Si} defect is less than 100nm in all three dimensions.¹⁹⁻²²

Firstly, we studied the optical and spin properties of the focused ion beam implanted V_{Si} defects using a home-built confocal fluorescence microscopy system.¹⁷ We used a 740nm laser for optical pumping of these defects as the wavelength of this laser is close to the optimum excitation wavelength of 770 nm.²³ We also used high quantum efficiency single photon detectors (ID Quantique ID120) in order to enhance the fluorescence collection of the V_{Si} defects. Fig. 1(a) shows the PL scan of a representative area of the 700 Si ions implanted V_{Si} defects array and stripes on the SiC surface (laser power 0.7mW). The spots are separated by ~2 μm. In order to identify the type of the defects, we firstly measured the room temperature PL spectrum of an ensemble of defects on the stripe after filtering the emission through a 900nm longpass filter (Fig1. (b)). The observed spectrum is in the near-infrared range and also similar to the previous measurement results of the PL spectrum of single and ensemble V_{Si} defects.^{3,5,7,17} Further, we measured the cryogenic temperature (5K) PL of the ensemble defects on the stripe with a cryogenic temperature confocal system (Montana Instruments Cryostation).^{17,24} As shown in Fig. 1(c), there are two spectral emission peaks (861.4nm, 916.5nm) which correspond to the two inequivalent lattice sites of the V_{Si} defects in 4H-SiC: V1 (861.4 nm) and V2 (916.3 nm) centers respectively.^{7,17,24}

The negatively charged V2 center in 4H-SiC is V_{Si} defect with spin 3/2. For spin manipulation of the implanted V_{Si} defects, we measured the continuous-wave ODMR of the ensemble V_{Si} defects on the stripe at room temperature. The radio frequency signal generated by a microwave source was first gated through a switch (ZASWA-2-50DR), and then amplified by a high power amplifier (ZHL-20W-13+). The radio frequency irradiation of V_{Si} defects was achieved with a 20μm width microwave stripline fabricated on the surface of sample by standard lithography techniques.¹⁷ The experiment was synchronized by a pulse generator (PulseBlaster PBESR-PRO-500). Since the ODMR contrast is expected to be less than one percent, we measured the ODMR signal by modulating the microwave drive amplitude (ON, OFF) which had a duty cycle of 0.5 and a half cycle duration of 2.8ms.^{7,9,17} Finally, the ODMR contrast, related to the change in PL, is calculated using the formula $\Delta PL = (\sum N(ON) - \sum N(OFF)) / \sum N(OFF)$.^{9,17} Fig 1(d) shows the results of the ODMR measurements of the V_{Si} ensemble defects and the red curve is a Lorentzian fit to the data. From

the fit, we obtain an estimated resonant frequency of 70.2 MHz, which is close to the zero field splitting of the V_{Si} center ($2D = 70$ MHz).

Next, we studied the single V_{Si} defect properties in the lowest dose (40 Si ions) implanted area. Fig. 2(a) shows the PL image of the V_{Si} defects array obtained from the silicon-implanted region at the SiC surface (laser power 0.7mW). The silicon ion dose was 40 ions per spot and the distance between spots was 2 μm . In order to identify a single V_{Si} defect, we measured the second-order autocorrelation function $g^2(\tau)$ using the Hanbury-Brown-Twiss (HBT) setup.¹⁷ Since the fluorescence count rate is low (13kcps), the effect of the background fluorescence has to be included in the evaluation of $g^2(\tau)$. The auto-correlation function $g^2(t)$ is corrected from normalized raw data $C_N(t)$ using the function $g^2(\tau) = (C_N(\tau) - (1 - \rho^2)) / \rho^2$, where $\rho = s/(s+b)$, and s and b are the signal and background count, respectively.^{5,9,17} In the experiment s and b was about 3 kcps and 2 kcps, respectively. A typical background-corrected $g^2(\tau)$ was shown in Fig. 2(b), and the red line was the fit according to the function $g^2(\tau) = 1 - a \cdot \exp(-|\tau|/\tau_1) + b \cdot \exp(-|\tau|/\tau_2)$, where a , b , τ_1 , τ_2 are fitting parameters. From the fit, we got $g^2(0) = 0.35 \pm 0.05$, which demonstrated it was a single V_{Si} defect.

The property of photostability is important for single photon sources in various quantum information applications.^{3,5} To this end, as shown in Fig 2(c), we measured the fluorescence intensity trace of a single V_{Si} defect with a sampling time of 100ms and 1mW laser power for a duration of 110 s. We could see that its count was very stable, and had no blinking or bleaching, which verified that it is a stable single photon source. Fig. 2(d) shows the emission intensity saturation curve of a single V_{Si} defect. The red line is a fit according to the formula $I(P) = I_s / (1 + P_0/P)$, where I_s is the maximum photon count rate, and P_0 is the saturation power, P is the laser power. Inferred from the fit, the maximum count rate I_s was about 13.0 kcps, and saturation power P_0 was about 0.48mW.

Efficient generation of defects in SiC is important for the coupling with photonics structure,⁹. In view of this, we present statistics of the distribution of the number of V_{Si} defects for 50 implanted spots by measuring defects $g^2(0)$ values, PL intensity and the mean counts of a single V_{Si} defect. The results are shown in Fig. 2(e), which agree with a Poisson distribution, $P_\lambda(k) = (\lambda^k / k!) / e^{-\lambda}$. Here λ is the average number of V_{Si} defects per spot and k is the number of V_{Si} centers actually formed in the spot. The average number of V_{Si} defects per spot, λ , was evaluated to be 1.56 by fitting the obtained distribution with a Poisson distribution. Thus the conversion yield of V_{Si} defects formation is evaluated to be about 3.9%. The conversion yield is comparable with the focused ion beam to generate the SiV center in diamond.^{20,22} Moreover, the number of the single V_{Si} defect was about 19, so the single V_{Si} defect generation efficiency was about 38%.

Finally, in order to systematically investigate the conversion yield of implanted Si^{++} ions to V_{Si} defects, we varied the ion doses on the sample from 40-700 cm^{-2} . The ion dose determined the number of silicon vacancies created during the implantation process. We measured the

fluorescence intensity across a $10 \times 10 \mu\text{m}^2$ region of constant implantation dose, and normalized to the mean counts per spot. Fig. 3(a) and (b) show typical confocal fluorescence image of an area of the 100 and 400 Si ions implanted V_{Si} defects array on the SiC surface, respectively. We observe that the PL emission intensity associated with V_{Si} centers increases with increasing silicon ion dose indicating an increase in the number of V_{Si} defects produced. As shown in Fig. 3(c), the average fluorescence rates per spot increases with increasing implantation dose (ions/spot). We found that when the implanted dose changes from 40 to 100 ions/spot, the mean counts per spot increased quickly. Then, it increased slowly with the implanted dose from 100 to 700 ions/spot. Finally, we normalized the mean counts per spot to the corresponding implanted ion number to get the conversion yield. As shown in Fig. 3(d), the conversion yield was almost same when the dose was 40 to 100 ions/spot, then it decreased as the dose increased from 100 to 700 ions/spot. This reduced yield might result from the accumulation of lattice damage and charged defects in SiC lattice, similar to what was observed in SiV centers in diamond.²⁰

In conclusion, we present a method for scalable and maskless generation of arrays of silicon vacancy centers in SiC using focused Si^{++} ion beam technology. The measured PL spectrum and ODMR of defect spin ensembles prove that the created defect centres are mostly the V_{Si} defect spins. Then we investigated the fluorescence properties of a single V_{Si} defect and found that it is a photostable single photon source with a saturation count rate of up to 13kcps. Finally, we found that the conversion yield of Si^{++} ions to V_{Si} defects decreases for higher implantation doses. This method offers new possibilities for realizing photonics applications where there arises a need to place single or a few V_{Si} defect centers within a nanometre-scale region. The photonic structures that may take benefit of this new method are solid immersion lenses (SIL),³ nanopillars⁹ or photonic crystal structures,¹⁰ fibers,²² as well as waveguides.^{18,25} Single V_{Si} defects could also be incorporated into the intrinsic region of a SiC positive-intrinsic-negative (PIN) diode structure for single-photon emission²⁶ and also into opto-mechanical resonators.²⁷ It can also be used to generate dipolar coupled V_{Si} defect pairs facilitating the creation of quantum registers.^{28,29}

Acknowledgment. We thank Evan Toh and Andrew Yu for the discussion about nanofabrication. We acknowledge the support from Singapore National Research Foundation through a Singapore 2015 NRF fellowship grant (NRF-NRFF2015-03, NRF-RF2013-08), its Competitive Research Program (CRP Award No. NRF-CRP14-2014-02), A*STAR QTE Project and Singapore Ministry of Education tier 1 project RG176/15.

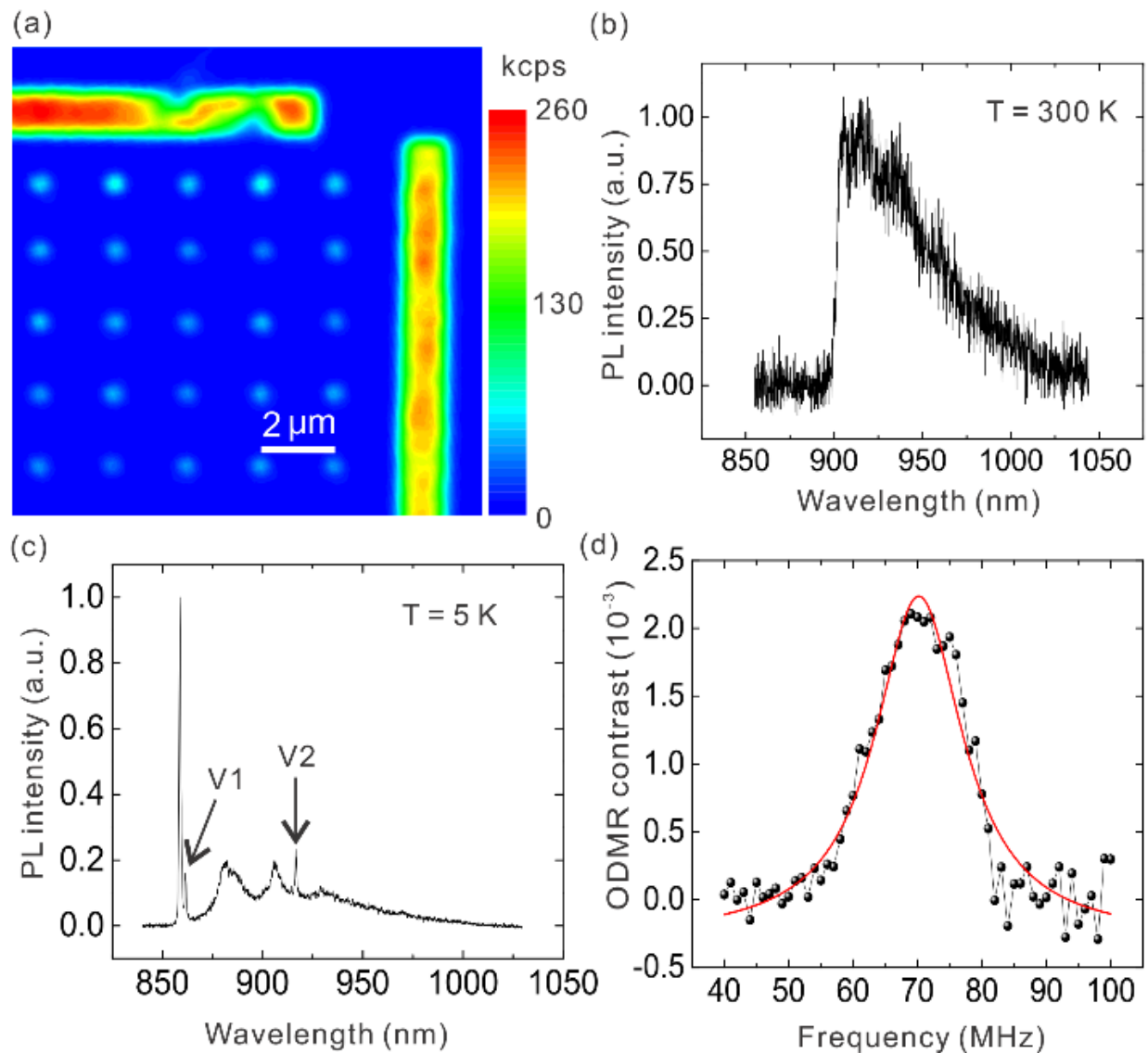


Figure1. Characterization of ensembles of defect. (a) Confocal fluorescence image for an area of the 700 Si ions implanted V_{Si} defects array and stripe on the SiC surface. The scale bar is $2\ \mu\text{m}$. (b) Room temperature PL spectrum measurement of the V_{Si} defects on the stripe. (c) The PL spectrum of the V_{Si} defects on the stripe at cryogenic temperature (5K). The two peaks correspond to the zero phonon lines of the V1 and V2 centers of the V_{Si} defects. (d) The room temperature ODMR detection of V_{Si} defects. The red line is the fit of the data.

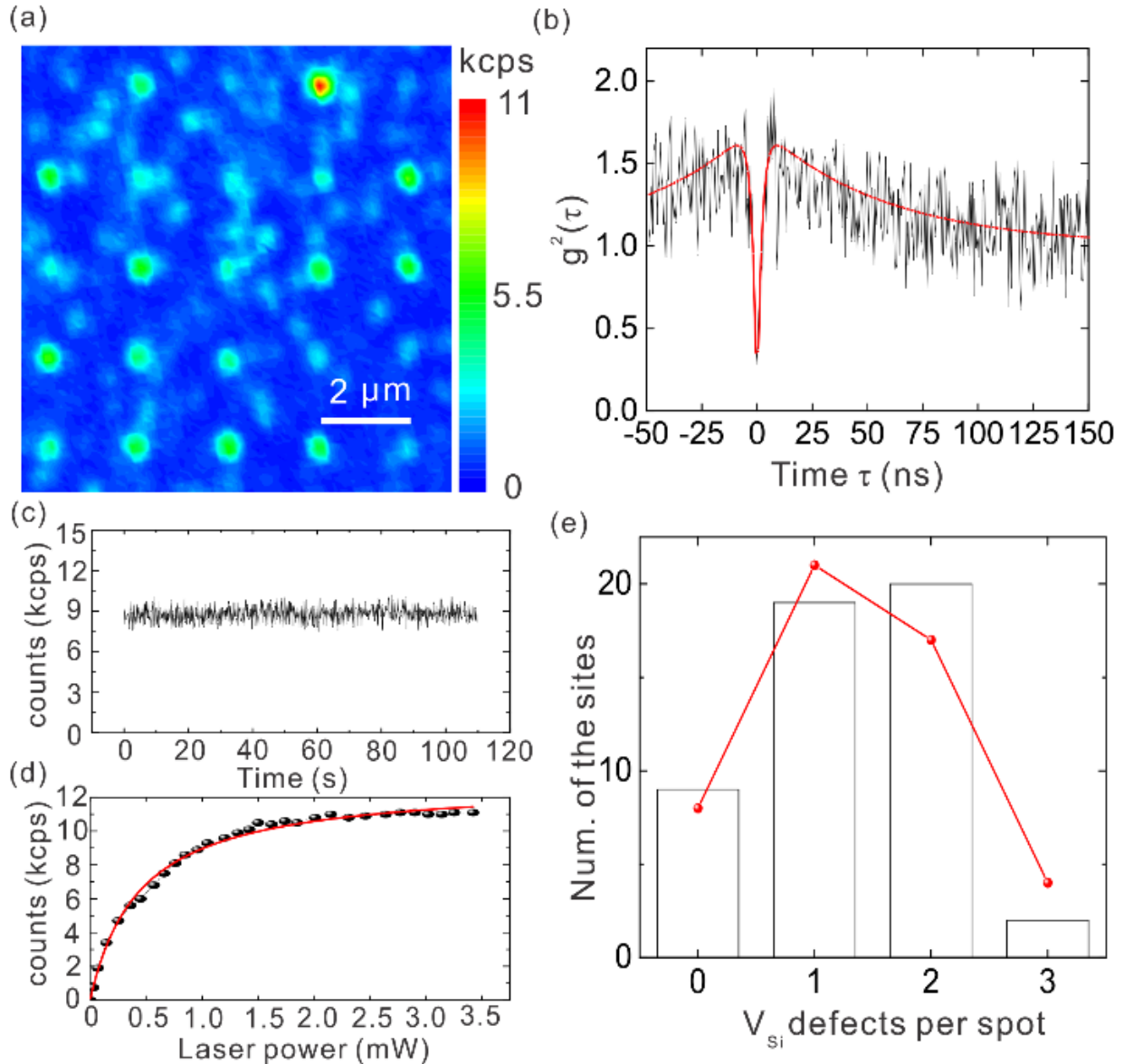


Figure 2. Single defect characterization. (a) Confocal fluorescence image for an area of the ^{40}Si ions implanted single V_{Si} defects array on the SiC surface. The scale bar is $2\mu\text{m}$. (b) Background-corrected second-order autocorrelation function of a single V_{Si} defect with $g^2(0) = 0.35 \pm 0.05$ under 0.65 mW of laser excitation power. (c) The fluorescence intensity trace of the single V_{Si} defect with a sampling time of 100ms and 1mW laser excitation power. (d) The fluorescence intensity measurements of a single V_{Si} defect emitter at different laser powers. (e) Statistics of the number of V_{Si} defects per implanted spot evaluated on 50 implanted sites. The data is fitted by a Poisson distribution (red curve).

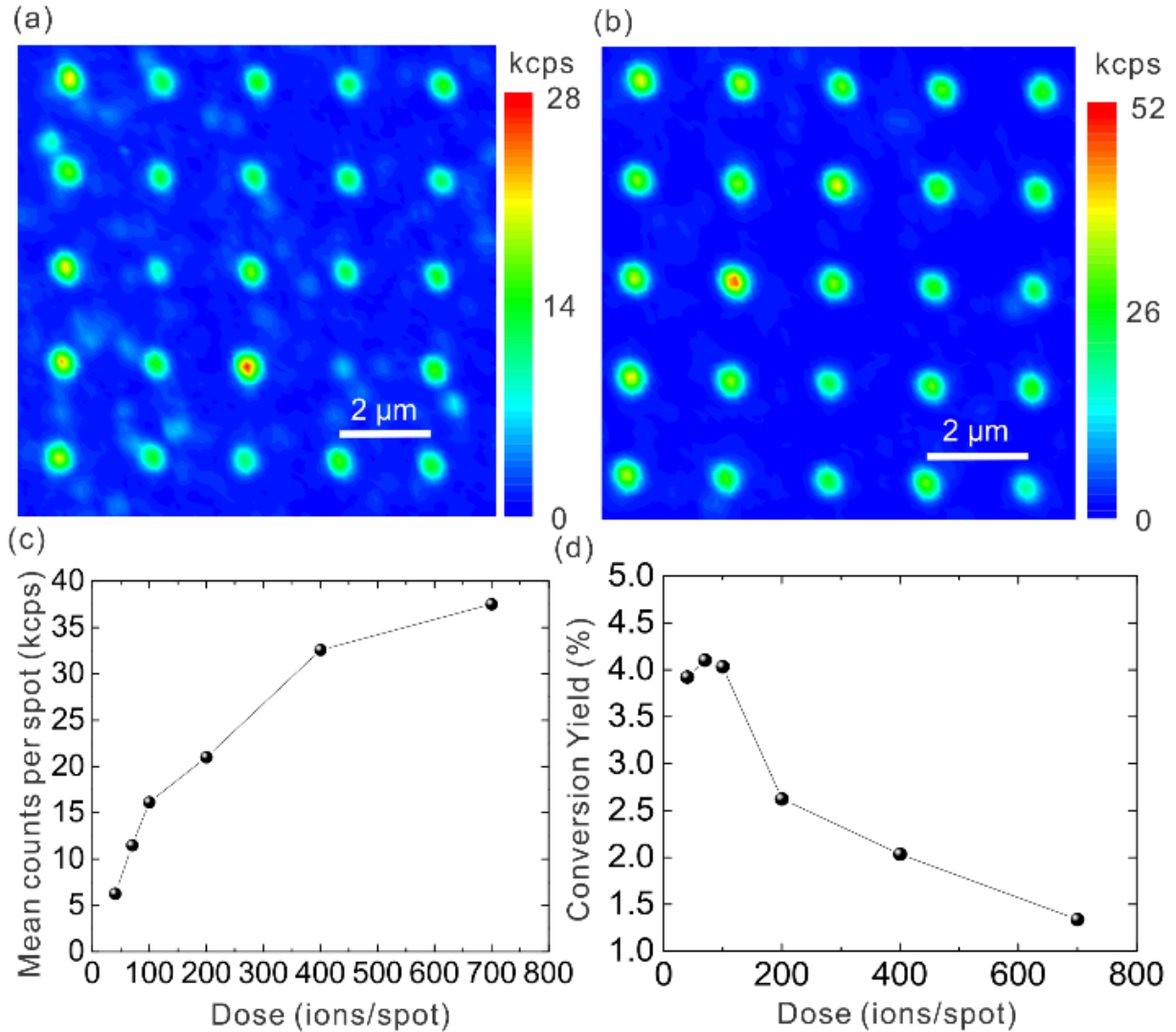


Figure 3. (a) and (b) Confocal fluorescence scans of a silicon carbide surface implanted with focused beams of Si^{++} ions corresponding to an applied dose of 100 and 400 respectively. The scale bar is $2\mu\text{m}$. (c) The mean fluorescence rates per spot as a function of Si^{++} ion dose (ions/spot). (d) The conversion yield of Si^{++} ions to V_{Si} defects as a function of Si^{++} ion dose (ions/spot).

References

1. Koehl, W. F.; Buckley, B. B.; Heremans, F. J.; Calusine, G.; Awschalom, D. D. Room Temperature Coherent Control of Defect Spin Qubits in Silicon Carbide. *Nature* **2011**, 479, 84-87.
2. Falk, A. L.; Buckley, B. B.; Calusine, G.; Koehl, W. F.; Dobrovitski, V. V.; Politi, A.; Zorman, C. A.; Feng, P. X. -L.; Awschalom, D. D. Polytype Control of Spin Qubits in Silicon Carbide. *Nature Commun.* **2013**, 4, 1819.
3. Widmann, M.; Lee, S. Y.; Rendler, T.; Son, N. T.; Fedder, H.; Paik, S.; Yang, L.-P.; Zhao, N.; Yang, S.; Booker, Denisenko, I.; Jamali, M.; Momenzadeh, S. A.; Gerhardt, I.; Ohshima, T.; Gali, A.;

Janzén, E.; Wrachtrup, J. Coherent Control of Single Spins in Silicon Carbide at Room Temperature. *Nat. Mater.* **2015**, *14*, 164-168.

4. Christle, D. J.; Falk, A. L.; Andrich, P.; Klimov, P. V.; Hassan, J. U.; Son, N. T.; Janzén, E.; Ohshima, T.; Awschalom, D. D. Isolated Electron Spins in Silicon Carbide with Millisecond Coherence Times. *Nat. Mater.* **2015**, *14*, 160-163.

5. Fuchs, F.; Stender, B.; Trupke, M.; Simin, D.; Pflaum, J.; Dyakonov, V.; Astakhov, G. V. Engineering Near-Infrared Single-Photon Emitters with Optically Active Spins in Ultrapure Silicon Carbide. *Nat. Commun.* **2015**, *6*, 7578.

6. Yang, L. P.; Burk, C.; Widmann, M.; Lee, S. Y.; Wrachtrup, J.; Zhao, N. Electron spin decoherence in silicon carbide nuclear spin bath. *Phys. Rev. B* **2014**, *90*, 241203(R).

7. Carter, S. G.; Soykal, Ö. O.; Dev, P.; Economou, S. E.; Glaser, E. R. Spin coherence and echo modulation of the silicon vacancy in 4 H-SiC at room temperature. *Phys. Rev. B* **2015**, *92*, 161202(R).

8. Klimov, P. V.; Falk, A. L.; Christle, D. J.; Dobrovitski, V. V.; Awschalom, D. D. Quantum entanglement at ambient conditions in a macroscopic solid-state spin ensemble. *Sci. Adv.* **2015**, *1*, e1501015.

9. Radulaski, M.; Widmann, M.; Niethammer, M.; Zhang, J. L.; Lee, S. Y.; Rendler, T.; Lagoudakis, K. G.; Son, N. Tien; Janzen, E.; Ohshima, T.; Wrachtrup, J. Scalable Quantum Photonics with Single Color Centers in Silicon Carbide. *arXiv*. **2016**, [1612.02874](https://arxiv.org/abs/1612.02874).

10. Bracher, D. O., Zhang, X. Y.; Hu, E. L. Selective Purcell enhancement of two closely linked zero-phonon transitions of a silicon carbide color center. *arXiv* **2016**, 1609.03918.

11. Calusine, G.; Politi, A.; Awschalom, D. D. Cavity-Enhanced Measurements of Defect Spins in Silicon Carbide. *Phys. Rev. Applied* **2016**, *6*, 014019.

12. Gruber, A.; Dräbenstedt, A.; Tietz, C.; Fleury, L.; Wrachtrup, J.; Von Borczyskowski, C. Scanning Confocal Optical Microscopy and Magnetic Resonance on Single Defect Centers. *Science* **1997**, *276*, 2012-2014.

13. Simin, D.; Kraus, H.; Sperlich, A.; Ohshima, T.; Astakhov, G. V.; Dyakonov, V. Long-Lived Quantum Memory in Silicon Carbide with Natural Isotope Abundance. *arXiv* **2016**, 1602.05775.

14. Simin, D.; Fuchs, F.; Kraus, H.; Sperlich, A.; Baranov, P. G.; Astakhov, G. V.; Dyakonov, V. High-Precision Angle-Resolved Magnetometry with Uniaxial Quantum Centers in Silicon Carbide. *Phys. Rev. Applied* **2015**, *4*, 014009.

15. Niethammer, M.; Widmann, M.; Lee, S. Y.; Stenberg, P.; Kordina, O.; Ohshima, T.; Son, N. T.; Janzén, E.; Wrachtrup, J. Vector Magnetometry Using Silicon Vacancies in 4H-SiC Under Ambient Conditions. *Phys. Rev. Applied* **2016**, *6*, 034001.

16. Anisimov, A. N.; Simin, D.; Soltamov, V. A.; Lebedev, S. P.; Baranov, P. G.; Astakhov, G. V.; Dyakonov, V. Optical Thermometry Based on Level Anticrossing in Silicon Carbide. *Sci. Rep.* **2016**, *6*, 33301.
17. Wang, J. F.; Zhou, Y.; Zhang, X. M.; Liu, F. C.; Li, Y.; Li, K.; Liu, Z.; Wang, G. Z.; Gao, W. B. High-Efficiency Generation of Nanoscale Single Silicon Vacancy Defect Array in Silicon Carbide. *arXiv.* **2016**, 1610.03978.
18. Gao, W. B.; Imamoglu, A.; Bernien, H.; Hanson, R. Coherent Manipulation, Measurement and Entanglement of Individual Solid-State Spins Using Optical Fields. *Nat. Photon.* **2015**, *9*, 363-373.
19. Sipahigil, A.; Evans, R. E.; Sukachev, D. D.; Burek, M. J.; Borregaard, J.; Bhaskar, M. K.; Nguyen, C.; Pacheco, J.; Atikian, H.; Meuwly, C.; Camacho, R. M.; Jelezko, F.; Bielejec, E.; Park, H.; Lončar, M.; Lukin, M. D. An Integrated Diamond Nanophotonics Platform for Quantum-Optical Networks. *Science* **2016**, *354*, 847-850.
20. Schröder, T.; Trusheim, M. E.; Walsh, M.; Li, L.; Zheng, J.; Schukraft, M.; Pacheco, J. L.; Camacho, R.M.; Bielejec, E.S.; Sipahigil, A.; Evans, R. E.; Sukachev, D. D.; Nguyen, C. T.; Lukin, M.D.; Englund, D. Scalable Focused Ion Beam Creation of Nearly Lifetime-Limited Single Quantum Emitters in Diamond Nanostructures. *arXiv* 2016, 1610. 09492.
21. Tamura, S.; Koike, G.; Komatsubara, A.; Teraji, T.; Onoda, S.; McGuinness, L. P.; Rogers, L.; Naydenov, B.; Wu, E.; Yan, L.; Jelezko, F.; Ohshima, T.; Isoya, J.; Shinada, T.; Tani, T. Array of Bright Silicon-Vacancy Centers in Diamond Fabricated by Low-Energy Focused Ion Beam Implantation. *Appl. Phys. Exp.* **2014**, *7*, 115201.
22. Burek, M. J.; Meuwly, C.; Evans, R. E.; Bhaskar, M. K.; Sipahigil, A.; Meesala, S.; Sukachev, D. D.; Nguyen, C. T.; Pacheco, J. L.; Bielejec, E.; Lukin, M. D.; Lončar, M. A Fiber-Coupled Diamond Quantum Nanophotonic Interface. *arXiv* **2016**, 1612 05285.
23. Hain, T. C.; Fuchs, F.; Soltamov, V. A.; Baranov, P. G.; Astakhov, G. V.; Hertel, T.; Dyakonov, V. Excitation and Recombination Dynamics of Vacancy-Related Spin Centers in Silicon Carbide. *J. Appl. Phys.* **2014**, *115*, 133508.
24. Li, K.; Zhou, Y.; Rasmita, A.; Aharonovich, I.; Gao, W. B. Nonblinking Emitters with Nearly Lifetime-Limited Linewidths in CVD Nanodiamonds. *Phys. Rev. Applied* **2016**, *6*, 024010.
25. Lesik, M.; Spinicelli, P.; Pezzagna, S.; Happel, P.; Jacques, V.; Salord, O.; Rasser, B.; Delobbe, A.; Sudraud, P.; Tallaire, A.; Meijer, J.; Roch, J.-F. Maskless and Targeted Creation of Arrays of Colour Centres in Diamond Using Focused Ion Beam Technology. *Phys. Status Solidi A* **2013**, *210*, 2055.

26. Lohrmann, A.; Iwamoto, N.; Bodrog, Z.; Castelletto, S.; Ohshima, T.; Karle, T. J.; Gali, A.; Prawer, S.; McCallum, J. C.; Johnson, B. C. Single-Photon Emitting Diode in Silicon Carbide. *Nat. Commun.* **2015**, *6*, 7783.
27. Arcizet, O.; Jacques, V.; Siria, A.; Poncharal, P.; Vincent, P.; Seidelin, S. A Single Nitrogen-Vacancy Defect Coupled to a Nanomechanical Oscillator. *Nat. Phys.* **2011**, *7*, 879-883.
28. Neumann, P.; Kolesov, R.; Naydenov, B.; Beck, J.; Rempp, F.; Steiner, M.; Jacques, V.; Balasubramanian, G.; Markham, M. L.; Twitchen, D. J.; Pezzagna, S. Meijer, J.; Twamley, J. Jelezko, F.; Wrachtrup, J. Quantum Register Based on Coupled Electron Spins in a Room-Temperature Solid. *Nat. Phys.* **2010**, *6*, 249-253.
29. Dolde, F.; Jakobi, I.; Naydenov, B.; Zhao, N.; Pezzagna, S.; Trautmann, C.; Meijer, J.; Neumann, P.; Jelezko, F.; Wrachtrup, J. Room-Temperature Entanglement Between Single Defect Spins in Diamond. *Nat. Phys.* **2013**, *9*, 139-143.